

Separated Response Function Ratios in Exclusive, Forward π^\pm Electroproduction

G.M. Huber,¹ H.P. Blok,^{2,3} C. Butuceanu,¹ D. Gaskell,⁴ T. Horn,⁵ D.J. Mack,⁴ D. Abbott,⁴ K. Aniol,⁶ H. Anklin,^{7,4} C. Armstrong,⁸ J. Arrington,⁹ K. Assamagan,¹⁰ S. Avery,¹⁰ O.K. Baker,^{10,4} B. Barrett,¹¹ E.J. Beise,¹² C. Bochna,¹³ W. Boeglin,⁷ E.J. Brash,¹ H. Breuer,¹² C.C. Chang,¹² N. Chant,¹² M.E. Christy,¹⁰ J. Dunne,⁴ T. Eden,^{4,14} R. Ent,⁴ H. Fenker,⁴ E.F. Gibson,¹⁵ R. Gilman,^{16,4} K. Gustafsson,¹² W. Hinton,¹⁰ R.J. Holt,⁹ H. Jackson,⁹ S. Jin,¹⁷ M.K. Jones,⁸ C.E. Keppel,^{10,4} P.H. Kim,¹⁷ W. Kim,¹⁷ P.M. King,¹² A. Klein,¹⁸ D. Koltenuk,¹⁹ V. Kovaltchouk,¹ M. Liang,⁴ J. Liu,¹² G.J. Lolos,¹ A. Lung,⁴ D.J. Margaziotis,⁶ P. Markowitz,⁷ A. Matsumura,²⁰ D. McKee,²¹ D. Meekins,⁴ J. Mitchell,⁴ T. Miyoshi,²⁰ H. Mkrtchyan,²² B. Mueller,⁹ G. Niculescu,²³ I. Niculescu,²³ Y. Okayasu,²⁰ L. Pentchev,⁸ C. Perdrisat,⁸ D. Pitz,²⁴ D. Potterveld,⁹ V. Punjabi,¹⁴ L.M. Qin,¹⁸ P.E. Reimer,⁹ J. Reinhold,⁷ J. Roche,⁴ P.G. Roos,¹² A. Sarty,¹¹ I.K. Shin,¹⁷ G.R. Smith,⁴ S. Stepanyan,²² L.G. Tang,^{10,4} V. Tadevosyan,²² V. Tvaskis,^{2,3} R.L.J. van der Meer,¹ K. Vansyoc,¹⁸ D. Van Westrum,²⁵ S. Vidakovic,¹ J. Volmer,^{2,26} W. Vulcan,⁴ G. Warren,⁴ S.A. Wood,⁴ C. Xu,¹ C. Yan,⁴ W.-X. Zhao,²⁷ X. Zheng,⁹ and B. Zihlmann^{28,4}

(The Jefferson Lab F_π Collaboration)

¹University of Regina, Regina, Saskatchewan S4S 0A2, Canada

²VU university, NL-1081 HV Amsterdam, The Netherlands

³NIKHEF, Postbus 41882, NL-1009 DB Amsterdam, The Netherlands

⁴Thomas Jefferson National Accelerator Facility, Newport News, Virginia 23606

⁵Catholic University of America, Washington, DC 20064

⁶California State University Los Angeles, Los Angeles, California 90032

⁷Florida International University, Miami, Florida 33119

⁸College of William and Mary, Williamsburg, Virginia 23187

⁹Physics Division, Argonne National Laboratory, Argonne, Illinois 60439

¹⁰Hampton University, Hampton, Virginia 23668

¹¹Saint Mary's University, Halifax, Nova Scotia B3H 3C3 Canada

¹²University of Maryland, College Park, Maryland 20742

¹³University of Illinois, Champaign, Illinois 61801

¹⁴Norfolk State University, Norfolk, Virginia 23504

¹⁵California State University, Sacramento, California 95819

¹⁶Rutgers, The State University of New Jersey, Piscataway, New Jersey 08854

¹⁷Kyungpook National University, Daegu, 702-701, Republic of Korea

¹⁸Old Dominion University, Norfolk, Virginia 23529

¹⁹University of Pennsylvania, Philadelphia, Pennsylvania 19104

²⁰Tohoku University, Sendai, Japan

²¹New Mexico State University, Las Cruces, New Mexico 88003-8001

²²A.I. Alikhanyan National Science Laboratory, Yerevan 0036, Armenia

²³James Madison University, Harrisonburg, Virginia 22807

²⁴DAPNIA/SPhN, CEA/Saclay, F-91191 Gif-sur-Yvette, France

²⁵University of Colorado, Boulder, Colorado 80309

²⁶DESY, Hamburg, Germany

²⁷Massachusetts Institute of Technology, Cambridge, Massachusetts 02139

²⁸University of Virginia, Charlottesville, Virginia 22901

(Dated: November 2, 2021)

The study of exclusive π^\pm electroproduction on the nucleon, including separation of the various structure functions, is of interest for a number of reasons. The ratio $R_L = \sigma_L^- / \sigma_L^+$ is sensitive to isoscalar contamination to the dominant isovector pion exchange amplitude, which is the basis for the determination of the charged pion form factor from electroproduction data. A change in the value of $R_T = \sigma_T^- / \sigma_T^+$ from unity at small $-t$, to 1/4 at large $-t$, would suggest a transition from coupling to a (virtual) pion to coupling to individual quarks. Furthermore, the mentioned ratios may show an earlier approach to pQCD than the individual cross sections. We have performed the first complete separation of the four unpolarized electromagnetic structure functions above the dominant resonances in forward, exclusive π^\pm electroproduction on the deuteron at central Q^2 values of 0.6, 1.0, 1.6 GeV² at $W=1.95$ GeV, and $Q^2 = 2.45$ GeV² at $W=2.22$ GeV. Here, we present the L and T cross sections, with emphasis on R_L and R_T , and compare them with theoretical calculations. Results for the separated ratio R_L indicate dominance of the pion-pole diagram at low $-t$, while results for R_T are consistent with a transition between pion knockout and quark knockout mechanisms.

Measurements of exclusive meson production are a useful tool in the study of hadronic structure. Through these studies, one can discern the relevant degrees of freedom at different distance scales. In contrast to inclusive (e, e') or photoproduction measurements, the transverse momentum (size) of a scattering constituent and the resolution at which it is probed can be varied independently. Exclusive *forward pion* electroproduction is especially interesting, because by detecting the charge of the pion, even the flavor of the interacting constituents can be tagged. Finally, *ratios* of separated response functions can be formed for which nonperturbative corrections may partially cancel, yielding insight into soft-hard factorization at the modest photon virtuality, Q^2 , to which exclusive measurements will be limited for the foreseeable future.

The longitudinal response in exclusive charged pion electroproduction has several important applications. At low Mandelstam variable $-t$, it can be related to the charged pion form factor, $F_\pi(Q^2)$, [1] which is used to test non-perturbative models of this “positronium” of light quark QCD. In order to reliably extract F_π from electroproduction data, the isovector t -pole process should be dominant in the kinematic region under study. This dominance can be studied experimentally through the ratio of longitudinal $\gamma_L^* n \rightarrow \pi^- p$ and $\gamma_L^* p \rightarrow \pi^+ n$ cross sections. If the photon possessed definite isospin, exclusive π^- production on the neutron and π^+ production on the proton would be related to each other by simple isospin rotation and the cross sections would be equal [2]. A departure from $R_L \equiv \sigma_L^{\pi^-} / \sigma_L^{\pi^+} = \frac{|A_V - A_S|^2}{|A_V + A_S|^2} = 1$, where A_S and A_V are the respective isoscalar and isovector photon amplitudes, would indicate the presence of isoscalar backgrounds arising from mechanisms such as ρ meson exchange [3] or perturbative contributions due to transverse quark momentum [4]. Such physics backgrounds may be expected to be larger at higher $-t$ (due to the drop-off of the pion pole) or non-forward kinematics (due to angular momentum conservation). Because previous data are unseparated [5], no firm conclusions about possible deviations of R_L from unity were possible.

In the limit of small $-t$, where the photon is expected to couple to the charge of the pion, the transverse ratio $R_T \equiv \sigma_T^{\pi^-} / \sigma_T^{\pi^+}$ is expected to be near unity. With increasing $-t$, the photon starts to probe quarks rather than pions, and the charge of the produced pion acts as a tag on the flavor of the participating constituent. Applying isospin decomposition and charge symmetry invariance to s -channel knockout of valence quarks in the hard-scattering regime, Nachtmann [6] predicted the exclusive electroproduction π^- / π^+ ratio at sufficiently large $-t$ to be $\frac{\gamma_T^* n \rightarrow \pi^- p}{\gamma_T^* p \rightarrow \pi^+ n} = \left(\frac{e_d}{e_u}\right)^2 = \frac{1}{4}$. Previous unseparated π^- / π^+ data [5] trend to a ratio of 1/4 for $|t| > 0.6 \text{ GeV}^2$, but

with relatively large uncertainties.

In the transition region between low $-t$ (where a description of hadronic degrees of freedom in terms of effective hadronic Lagrangians is valid) and large $-t$ (where the degrees of freedom are quarks and gluons), t -channel exchange of a few Regge trajectories permits an efficient description of the energy dependence and the forward angular distribution of many real- and virtual-photon-induced reactions. The VGL Regge model [7, 8] has provided a good and consistent description of a wide variety of π^\pm photo- and electroproduction data above the resonance region. However, the model has consistently failed to provide a good description of $p(e, e' \pi^+) n$ σ_T data [9]. The VGL Regge model was recently extended [10, 11] by the addition of a hard deep inelastic scattering (DIS) process of virtual-photons off nucleons. The DIS process dominates the transverse response at moderate and high Q^2 , providing a better description of σ_T .

Exclusive π^\pm electroproduction has also been calculated in the handbag framework, where only one parton participates in the hard subprocess, and the soft physics is encoded in generalized parton distributions (GPDs). Pseudoscalar meson production, such as σ_T in exclusive π^\pm electroproduction which is not dominated by the pion pole term, has been identified as being especially sensitive to the chiral-odd transverse GPDs [12, 13]. The model of Refs. [13, 14] uses a modified perturbative approach based on GPDs, incorporating the full pion electromagnetic form factor and substantial contributions from the twist-3 transversity GPD, H_T .

We have performed a complete $L/T/LT/TT$ separation in exclusive forward π^\pm electroproduction from deuterium. Here, we present the L and T cross sections, with emphasis on R_L and R_T in order to better understand the dynamics of this fundamental inelastic process; the LT and TT interference cross sections will be presented in a future work. Because there are no practical free neutron targets, the ${}^2\text{H}(e, e' \pi^\pm) NN_s$ reactions (where N_s denotes the spectator nucleon) were used. In π^- / π^+ ratios, the corrections for nuclear binding and rescattering largely cancel.

The data were obtained in Hall C at the Thomas Jefferson National Accelerator Facility (JLab) as part of the two pion form factor experiments presented in detail in Ref. [9]. Except where noted, the experimental details and data analysis techniques are as presented in Ref. [9] for the ${}^1\text{H}(e, e' \pi^+) n$ data. Charged π^\pm were detected in the High Momentum Spectrometer (HMS) while the scattered electrons were detected in the Short Orbit Spectrometer (SOS). Given the kinematic constraints imposed by the available electron beam energies and the properties of the HMS and SOS magnetic spectrometers, deuterium data were acquired in the first experiment

for nominal (Q^2 , W , $\Delta\epsilon$) settings of (0.60, 1.95, 0.37), (1.00, 1.95, 0.32), (1.60, 1.95, 0.36), and in the second experiment of (2.45, 2.22, 0.27). The value $W=1.95$ GeV used in the first experiment is high enough to suppress most s -channel baryon resonance backgrounds, but this suppression should be even more effective in the second experiment. For each Q^2 setting, the electron spectrometer angle and momentum, as well as the pion spectrometer momentum, were kept fixed. To attain full coverage in ϕ , in most cases additional data were taken with the pion spectrometer at a slightly smaller and at a larger angle than the \vec{q} -vector direction for the high ϵ settings. At low ϵ , only the larger angle setting was possible. The HMS magnetic polarity was reversed between π^+ and π^- running, with the quadrupoles and dipole magnets cycled according to a standard procedure. Kinematic offsets in spectrometer angle and momentum, as well as in beam energy, were previously determined using elastic e^-p coincidence data taken during the same run, and the reproducibility of the optics checked [9].

The potential contamination by electrons when the pion spectrometer is set to negative polarity, and by protons when it is set to positive polarity, introduces some differences in the π^\pm data analyses which were carefully examined. For most negative HMS polarity runs, electrons were rejected at the trigger level by a gas Čerenkov detector containing C_4F_{10} . The beam current was significantly reduced during π^- running to minimize the inefficiency due to electrons passing through the gas Čerenkov within ≈ 100 ns after a pion has traversed the detector, causing the pion to be misidentified as an electron. A Čerenkov blocking correction (1-15%) was applied to the π^- data using the measured electron rates combined with the effective time window of the gas Čerenkov ADC, the latter determined from data where the Čerenkov was not in the trigger. A cut on particle speed ($v/c > 0.95$), calculated from the time-of-flight difference between two scintillator planes in the HMS detector stack, was used to separate π^+ from protons. Additionally in the second experiment, an aerogel Čerenkov detector was used to separate protons and π^+ for central momenta above 3 GeV/ c . A correction for the number of pions lost due to pion nuclear interactions and true absorption in the HMS exit window and detector stack of 4.5-6% was applied. For further details, see Ref. [9].

Because the π^- data are typically taken at higher HMS detector rates than the π^+ data, a good understanding of rate-dependent efficiency corrections was required. An improved high rate tracking algorithm was implemented, resulting in high rate tracking inefficiencies of 2-9% for HMS rates up to 1.4 MHz. Liquid deuterium target boiling corrections of 4.7%/100 μA were determined for the horizontal-flow target used in the first experiment. The vertical-flow target and improved beam raster used in the second experiment resulted in a negligible boiling correction for those data. The experimental yields were also

corrected for dead time (1-11%).

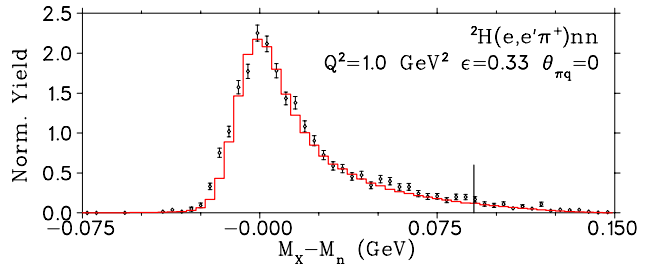


FIG. 1. (Color online) Missing mass of the undetected nucleon calculated as quasi-free pion electroproduction for a representative π^+ setting. The diamonds are experimental data, and the red line is the quasi-free Monte Carlo simulation. The vertical line indicates the M_X cut upper limit.

Kinematic quantities such as t and missing mass M_X were reconstructed as quasi-free pion electroproduction, $\gamma^*N \rightarrow \pi^\pm N'$, where the virtual-photon interacts with a nucleon at rest. The former is calculated using $t = (p_{\text{target}} - p_{\text{recoil}})^2$, which can differ from $(p_\gamma - p_\pi)^2$ due to Fermi motion and radiation. Missing mass cuts were then applied to select the exclusive final state (Fig. 1). Because of Fermi motion in the deuteron, this cut is taken wider than for a hydrogen target. Real and random coincidences were isolated with a coincidence time cut of ± 1 ns. Background from aluminum target cell walls (2-4% of the yield) and random coincidences ($\sim 1\%$) were subtracted from the charge-normalized yields on a bin by bin basis.

The virtual-photon cross section can be expressed in terms of contributions from transversely and longitudinally polarized photons, and interference terms,

$$2\pi \frac{d^2\sigma}{dtd\phi} = \frac{d\sigma_T}{dt} + \epsilon \frac{d\sigma_L}{dt} + \sqrt{2\epsilon(1+\epsilon)} \frac{d\sigma_{LT}}{dt} \cos\phi \quad (1) \\ + \epsilon \frac{d\sigma_{TT}}{dt} \cos 2\phi.$$

Here, $\epsilon = \left(1 + 2\frac{|\vec{q}|^2}{Q^2} \tan^2 \frac{\theta}{2}\right)^{-1}$ is the virtual-photon polarization, where \vec{q} is the three-momentum transferred to the quasi-free nucleon, θ is the electron scattering angle, and ϕ is the azimuthal angle between the scattering and the reaction plane.

For each charge state, the data for $d^2\sigma/dtd\phi$ were binned in t and ϕ and the individual components in Eqn. 1 determined from a simultaneous fit to the ϕ dependence of the measured cross sections at two values of ϵ . The separated cross sections are determined at fixed values of W , Q^2 , common for both high and low values of ϵ . Because the acceptance covers a range in W and Q^2 , the measured cross sections, and hence the separated response functions, represent an average over this range. They are determined at the average values (for both ϵ points together), $\overline{Q^2}$, \overline{W} , which are different for each t

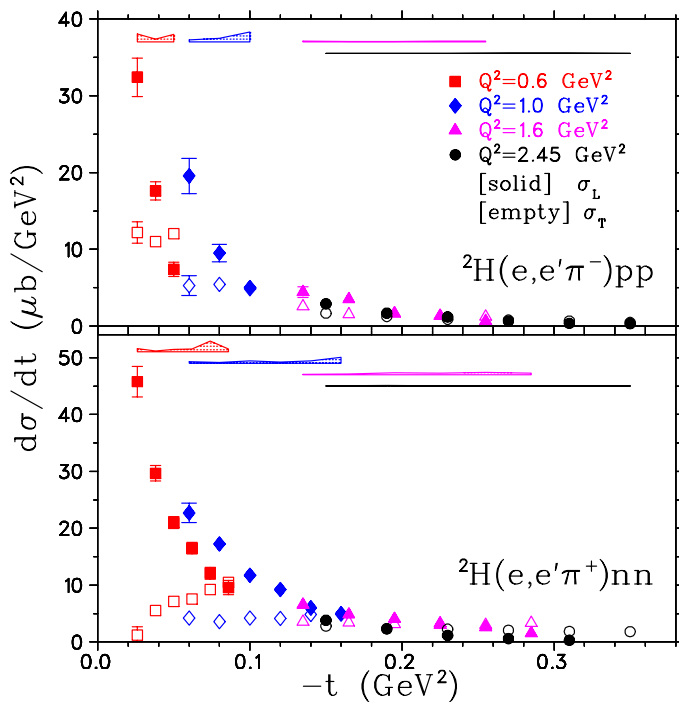


FIG. 2. (Color online) Separated exclusive π^\pm electroproduction cross sections from deuterium. Because the data were taken at different values of \overline{W} , all cross sections were scaled to a value of $W = 2.0$ GeV according to $1/(W^2 - M^2)$. The error bars indicate statistical and uncorrelated systematic uncertainties in both ϵ and $-t$, combined in quadrature. The shaded error bands indicate the model-dependence of σ_L . The σ_T model-dependence (not shown) is smaller.

bin. The experimental cross sections were calculated by comparing the experimental yields to a Monte Carlo simulation of the experiment. The simulation uses a quasi-free $N(e, e'\pi^\pm)N'$ model, where the struck nucleon carries Fermi momentum, but the events are reconstructed in the same manner as the experimental data, i.e. assuming the target is a nucleon at rest. The Monte Carlo includes a detailed description of the spectrometers, multiple scattering, ionization energy loss, pion decay, and radiative processes.

The separated cross sections, σ_L and σ_T , are shown in Fig. 2. Even if π^+ production on ${}^2\text{H}$ occurs only on the proton, the deuterium cross section cannot be directly connected to the free ${}^1\text{H}$ cross section because the Monte Carlo cross-section model ignores off-shell effects and averages over the nucleon momentum distribution in ${}^2\text{H}$. The uncertainties in the separated cross sections have both statistical and systematic sources. The statistical uncertainty in $\sigma_T + \epsilon\sigma_L$ is 5-10% for π^- settings, and more uniformly near 5% for π^+ settings. Systematic uncertainties that are uncorrelated between high and low ϵ points are amplified by a factor of $1/\Delta\epsilon$ in the L/T separation. This uncertainty ($\sim 1.3\%/\Delta\epsilon$) is dominated by

uncertainties in the spectrometer acceptance, uncertainties in the efficiency corrections due to Čerenkov trigger blocking and analysis cuts, and the Monte Carlo model-dependence. Scale systematic uncertainties of $\sim 3\%$ (not shown in the figure) propagate directly into the separated cross sections. They are dominated by uncertainties in the radiative corrections, pion decay and pion absorption corrections, and the tracking efficiencies. The systematic uncertainty due to the simulation model and the applied M_X cut (model-dependence) was estimated by extracting new sets of $L/T/LT/TT$ cross sections with alternate models and tighter M_X cuts.

In the σ_L response of Fig. 2, the pion pole is evident by the sharp rise at small $-t$. π^- and π^+ are similar, and the data at different Q^2 follow a nearly universal curve versus t , with only a weak Q^2 -dependence. The T responses are flatter versus t .

Finally, π^-/π^+ ratios of the separated cross sections were formed to cancel nuclear binding and rescattering effects. Many experimental normalization factors cancel to a high degree in the ratio (acceptance, target thickness, pion decay and absorption in the detectors, radiative corrections, etc.). The principal remaining uncorrelated systematic errors are in the tracking inefficiencies, target boiling corrections, and Čerenkov blocking corrections.

Fig. 3 shows the first experimental determination of R_L . The ratio is approximately 0.8 near $-t_{\min}$ at each Q^2 setting, as predicted in the large N_c limit calculation of Ref. [15]. The data are generally lower than the predictions of the pion-pole dominated models [8, 10, 11]. Under the naive assumption that the isoscalar and isovector amplitudes are real, $R_L = 0.8$ gives $A_S/A_V = 0.06$. This is relevant for the extraction of the pion form factor from electroproduction data, which uses a model including some isoscalar background. This result is qualitatively in agreement with the findings of our pion form factor analyses [1, 16], which found evidence of a small additional contribution to σ_L not taken into account by the VGL Regge Model in our $Q^2 = 0.6 - 1.6$ GeV 2 data at $W = 1.95$ GeV, but little evidence for any additional contributions in our $Q^2 = 1.6 - 2.45$ GeV 2 data at $W = 2.2$ GeV. The main conclusion to be drawn is that pion exchange dominates the forward longitudinal response even $\sim 10 m_\pi^2$ away from the pion pole.

Also in Fig. 3 are the first R_T results in electroproduction. At $Q^2=0.6, 1.0$ GeV 2 , R_T drops rapidly and given the small t -range covered, it is not apparent if this drop is due to t or Q^2 -dependence. However, the values at $Q^2=1.6$ and 2.45 GeV 2 overlap, suggesting that R_T is primarily a function of $-t$, dropping from about 0.6 at $-t=0.15$ to about 0.3 at $-t=0.3$ GeV 2 . Interestingly, photoproduction data in this t -range [17] give similar values. It is noteworthy that the unseparated data of Ref. [5] reach a value of 0.3 at a much higher value of $-t$. A value of $-t=0.3$ GeV 2 seems quite low for quark-charge

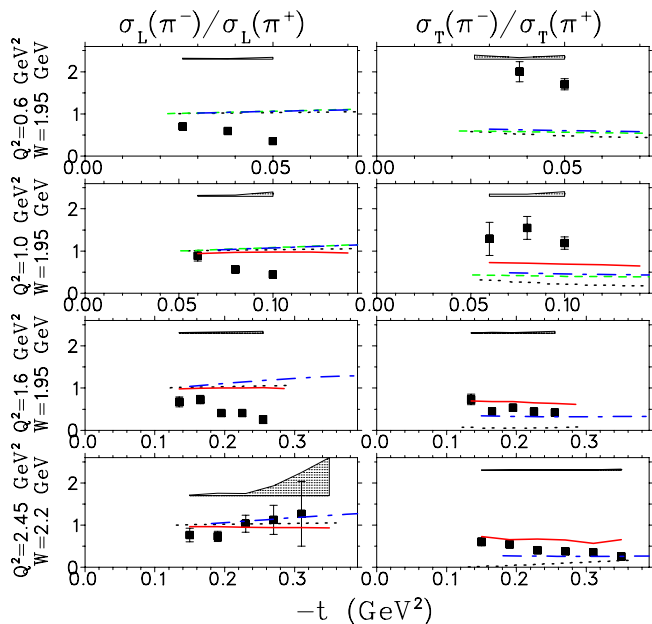


FIG. 3. (Color online) The ratios R_L and R_T versus $-t$ for four Q^2 settings. The error bars include statistical and uncorrelated systematic uncertainties. The model-dependences of the ratios are indicated by the shaded bands. The dotted black curves are predictions of the VGL Regge model [8] using the values $\Lambda_\pi^2 = 0.394, 0.411, 0.455, 0.491$ GeV², as determined from fits to our ¹H data [1], and the solid red curves are predictions by Goloskokov and Kroll [14], both models calculated at the same \bar{W} , Q^2 as the data. The dashed green curves are predictions by Kaskulov and Mosel [10], and the dot-dashed blue curves are the predictions by Vrancx and Rycebusch [11], both models calculated at the nominal kinematics.

scaling arguments to apply directly. This might indicate the partial cancellation of soft QCD corrections in the transverse π^-/π^+ ratios. Previous photoproduction measurements of R_T have hinted at quark-partonic behavior, but such non-forward, $Q^2 = 0$ measurements are inherently more difficult to interpret due to sea quark and u -channel contributions. Indeed, the photoproduction measurements at sufficiently high $-t$ first dip down toward 1/4 then *increase* at backward angles [18]. The models of Refs. [7, 10, 11] do not accurately predict R_T at $-t_{\min}$, although [11] does much better at higher $-t$. The Goloskokov-Kroll GPD-based model is in reasonable agreement, but the parameters in this model are optimized for small skewness ($\xi < 0.1$) and large $W > 4$ GeV. The application of this model to the kinematics of our data requires a substantial extrapolation and one should be cautious in this comparison. Indeed, although the model does a reasonable job at predicting the π^-/π^+ ratios, the agreement of the model with σ_T is not good [14]. Further theoretical work is clearly needed to investigate alternative explanations of the observed ratios.

To summarize, our data for R_L trend toward unity at low $-t$, indicating the dominance of isovector processes in forward kinematics, which is relevant for the extraction of the pion form factor from electroproduction data [1, 16, 19]. The evolution of R_T with $-t$ shows a rapid fall off consistent with s -channel quark knockout. Since R_T is not dominated by the pion pole term, this observable is likely to play an important role in future transverse GPD programs. Further work is planned after the completion of the JLab 12 GeV upgrade, including complete separations at $Q^2=5-10$ GeV² over a larger range of $-t$ [20].

The authors thank Drs. Goloskokov and Kroll for the unpublished model calculations at the kinematics of our experiment, and Drs. Guidal, Laget, and Vanderhaeghen for modifying their computer program for our needs. This work is supported by DOE and NSF (USA), NSERC (Canada), FOM (Netherlands), NATO, and NRF (Rep. of Korea). Additional support from Jefferson Science Associates and the University of Regina is gratefully acknowledged. At the time these data were taken, the Southeastern Universities Research Association (SURA) operated the Thomas Jefferson National Accelerator Facility for the United States Department of Energy under contract DE-AC05-84150.

-
- [1] G.M. Huber, *et al.*, Phys. Rev. C **78** (2008) 045203.
 - [2] A.M. Boyarski, *et al.*, Phys. Rev. Lett. **21** (1968) 1767.
 - [3] M. Vanderhaeghen, M. Guidal, and J.-M. Laget, Phys. Rev. C **57** (1998) 1454.
 - [4] C.E. Carlson, J. Milana, Phys. Rev. Lett. **65** (1990) 1717.
 - [5] P. Brauel, *et al.*, Z. Physik **C 3** (1979) 101; M. Schaedlich, Dissertation des Doktorgrades, Universitaet Hamburg, 1976, DESY F22-76/02 November 1976.
 - [6] O. Nachtmann, Nucl. Phys. **B115** (1976) 61.
 - [7] M. Guidal, J.-M. Laget, M. Vanderhaeghen, Nucl. Phys. **A 627** (1997) 645.
 - [8] M. Vanderhaeghen, M. Guidal, J.-M. Laget, Phys. Rev. C **57** (1998) 1454.
 - [9] H.P. Blok, *et al.*, Phys. Rev. C **78** (2008) 045202.
 - [10] M.M. Kaskulov, U. Mosel, Phys. Rev. C **81** (2010) 045202.
 - [11] T. Vrancx, J. Rycebusch, Phys. Rev. C **89** (2014) 025203.
 - [12] S. Ahmad, G.R. Goldstein, S. Liuti, Phys. Rev. D **79** (2009) 054014.
 - [13] S.V. Goloskokov, P. Kroll, Eur. Phys. J. C **65** (2010) 137.
 - [14] S.V. Goloskokov, P. Kroll, Eur. Phys. J. A **47** (2011) 112; and Private Communication, 2013.
 - [15] L.L. Frankfurt, M.V. Polyakov, M. Strikman, M. Vanderhaeghen, Phys. Rev. Lett. **84** (2000) 2589.
 - [16] J. Volmer, *et al.*, Phys. Rev. Lett. **86** (2001) 1713.
 - [17] P. Heide, *et al.*, Phys. Rev. Lett. **21** (1968) 248.
 - [18] L.Y. Zhu, *et al.*, Phys. Rev. Lett. **91** (2003) 022003; Phys. Rev. C **71** (2005) 044603.
 - [19] T. Horn, *et al.*, Phys. Rev. Lett. **97** (2006) 192001.
 - [20] G.M. Huber, D. Gaskell, *et al.*, Jefferson Lab Experiment

E12-06-101; T. Horn, G.M. Huber, *et al.*, Jefferson Lab

Experiment E12-07-105.